J Mater Sci (2017) 52:11179–11190

Macroporous Materials

Single-source macroporous hybrid materials by melt-shear organization of core–shell particles

Steffen Vowinkel[1], Frank Malz[2], Karsten Rode[2], and Markus Gallei[1,*]

[1] *Ernst-Berl-Institute for Chemical Engineering and Macromolecular Science, Technische Universität Darmstadt, Alarich-Weiss-Str. 4, 64287 Darmstadt, Germany*

[2] *Fraunhofer-Institut für Betriebsfestigkeit und Systemzuverlässigkeit LBF, Schlossgartenstr. 6, 64289 Darmstadt, Germany*

Received: 15 December 2016
Accepted: 3 February 2017
Published online: 10 February 2017

ABSTRACT

The preparation of porous materials is an interesting field for a huge variety of potential applications. Herein we report an efficient and convenient strategy for the creation of inverse colloidal crystal structures based on soft core/shell polymer particle templating. This single-source strategy is based on starved-feed emulsion polymerization of hybrid core/shell particles consisting of a poly(methyl methacrylate-*co*-allyl methacrylate) (P(MMA-*co*-ALMA)) core and a poly(ethyl acrylate-*co*-(3-methacryloxypropyl-trimethoxysilane)) (PEA-*co*-PMEMO) shell. The resulting monodisperse particles are analyzed with respect to their size and distribution by transmission electron microscopy (TEM) and dynamic light scattering (DLS) measurements. The hybrid monodisperse core/shell particles can be aligned to a colloidal crystal by using the convenient melt-shear organization technique. As a result, free-standing and crack-free hybrid polymer colloidal crystal films are accessible without the need of any solvent or dispersion medium. The processing step is investigated regarding different parameters comprising temperature and pressure for the influence on the colloidal crystal film formation. Furthermore, resulting core/shell ratio is tailored by starved-feed emulsion polymerization conditions, since the ratio affects the quality of the porous structure after thermal treatment of colloidal crystal films. The incorporation of alkoxysilane-containing monomers offers a unique crosslinking strategy that yields mechanically robust and thermally stable films. Due to the increased stability, a removal of PMMA cores is possible by thermal treatment of the templating colloidal crystal films leading to almost isoporous free-standing hybrid materials as determined by thermogravimetric analysis (TGA) and scanning electron microscopy (SEM).

Address correspondence to E-mail: m.gallei@mc.tu-darmstadt.de

DOI 10.1007/s10853-017-0891-2

Introduction

Hierarchically ordered materials with various architectures in the nanometer scale are well known from nature. Over the last decades, scientists have spurred intensive research in order to mimic and produce similar structures [1]. Such materials feature excellent structural control making them interesting for a huge variety of applications in the field of optical, electrical, magnetic and chemical sensors. If these hierarchically structured materials additionally bear functional moieties, they can be triggered by external stimuli [2–5]. In general, multifunctional artificial structures can either be pure organic, inorganic or hybrid, *i.e.*, a combination of inorganic and organic units. Moreover, the fabrication of hierarchically structured (meso)porous materials led to the combination of, *e.g.*, hollow spheres, nanowires, nanorods, nanotubes, fibers, membranes or 3D-ordered porous materials. Some recent strategies focus on guiding the self-assembly of block copolymers [6, 7]. Within this field, there are different approaches for the preparation of ceramic materials, nanocomposites included. For deeper insights, readers are referred to contributions by Orilall and Wiesner [8] and other authors [9–13]. Hierarchical colloidal architectures, especially inverse opals with adjustable dimensions, have gained considerable attention due to their tremendous potential for various applications in catalysis, separation, sensors, optics and biomedicine [14, 15]. Different templating strategies have been applied for controlling shape and size of the final (porous) materials after removal of the sacrificial structure [16–21]. In particular hard templating is a versatile technique for the formation of hollow micro- and nanostructures [22]. In contrast, polymer-based templating strategies for the preparation of advanced ceramics are known as *soft templating*. The self-assembly of preceramic core/shell architectures is a versatile method for the preparation of 3D hierarchically ordered ceramic materials via pyrolysis. This technique is based on tailor-made micro- and nanoparticles with the intrinsic capability of colloidal crystallization, which is particularly interesting for optical applications [23]. In general, colloidal crystals can be prepared by various techniques such as particle deposition or spin coating of respective dispersion [24–26]. Moreover, the precise arrangement of polymer particles can be improved in flow fields by, *e.g.*, combinations of melting and shear-ordering methods leading to so-called polymer opal films [27, 28]. This technique—also known as melt-shear organization—uses core–shell particles and has the major advantage of solvent- and dispersion-free processing. This technique involves the compression of monodisperse hard core particles covered by a comparably soft shell. These particles are compressed between the plates of a moderately hot press and the hard core particles can merge into the colloidal crystal structure due to softening of the soft polymer shell. In recent years, this technique has been optimized by using a combination of extrusion, rolling and edge-induced rotational shearing steps, providing access to almost perfectly ordered colloidal crystal films on the multi-meter length scale [29–32]. Thus, large-area self-supporting opal films could be obtained. Compared to above mentioned methods for the preparation of polymeric opal films, this strategy is fast yielding polymer films in one single processing step. In more recent studies, optical properties of opal materials addressable by external triggers, *e.g.*, temperature, ionic strength, light, or by applying an electrical field or mechanical stress attracted enormous attention in the scientific community [33–40]. However, this particle organization technique was limited to pure organic core/shell particle architectures. Only recently, the usability of inorganic core particles featuring a soft and meltable shell for the melt-shear organization technique was reported. Exemplarily, smart inverse opal films with unprecedented optical properties or carbonaceous inverse opals were accessible by using silica as core materials [41, 42].

Within the present study, we focus on a convenient single-source precursor route for porous materials based on hybrid core/shell particles. The monodisperse core/shell particles are synthesized via starved-feed emulsion polymerization, which offers excellent control over particle size, core/shell ratio and architecture. The core is made of PMMA, while the hybrid shell consists of poly(ethyl acrylate) (PEA) and poly(3-methacryloxypropyl-trimethoxysilane) (PMEMO). The soft PEA maintains the melt-shearing capabilities, while PMEMO enables polysiloxanes crosslinking during processing and serves as source for the final SiOC-based ceramic material. The hybrid crosslinking strategy increases stability of the polymer matrix for subsequent removal of PMMA cores by thermal treatment. The essential balance between core/shell ratio, MEMO content and processing steps

is investigated in order to produce hierarchically ordered porous materials in one single step.

Experimental

Materials

Methyl methacrylate (MMA) and allyl methacrylate (ALMA) were obtained from Fisher Scientific, ethyl acrylate (EA) from BASF SE and Dowfax 2A1 from Dow Chemicals. All other chemicals were obtained from Sigma-Aldrich. Prior to use in emulsion polymerization, the inhibitors were removed from the monomers by passing the monomers through a basic alumina column.

Synthesis

Synthesis of PMMA-co-ALMA core particles

Hybrid core/shell particles were synthesized in a 1 L double-wall reactor equipped with stirrer and reflux condenser at 75 °C under argon. Starting with a solution of 440 g water, 3.6 g methyl methacrylate, 0.4 g allyl methacrylate and 30 mg Triton X-405 (or 35 mg SDS), a mixture of 50 mg sodium bisulfite, 150 mg sodium persulfate and 50 mg sodium bisulfate is added in this sequence to initiate seed particle growth. After 15 min, a monomer emulsion is added with a flow rate of 1.2 mL min^{-1}. The monomer emulsion consists of 72 g water, 50.4 g MMA, 5.6 g ALMA, 170 mg sodium dodecyl sulfate (SDS), 200 mg KOH and 120 mg Dowfax 2A1.

Synthesis of PMMA-co-ALMA@PEA-co-PEMO core/shell particles

The previously described polymerization of the core particles was continued for different shell compositions as compiled in Table 1. The core particle dispersion is buffered with 5 mL of 0.1 M phosphate buffer. After 15 min, the monomer emulsion for the shell material is continuously added.

Synthesis of PMEMO-co-PEA particles for TGA investigations

For synthesis of pure PEA-*co*-PMEMO particles, a solution of 440 g water, 2.6 g MMA, 1.4 g ALMA and 200 mg SDS was added for seed particle synthesis. The polymerization was initiated with a mixture of 50 mg sodium bisulfite, 150 mg sodium persulfate and 50 mg sodium bisulfate added in this sequence. After 15 min, a monomer emulsion is added with a flow rate of 1.2 mL min^{-1}. The monomer emulsion consists of 72 g water, 36.4 g EA, 19.6 g MEMO, 170 mg SDS, 120 mg Dowfax 2A1 and 1.5 mL of 0.1 M phosphate buffer (pH 7.1).

Table 1 Composition of monomer emulsions for shell synthesis

Particles for melt-shear processing PMMA-*co*-ALMA@PEA-*co*-PMEMO	30 g water 13.5 g EA 13.5 g MEMO 75 mg SDS 75 mg Dowfax 2A1 1 mL phosphate buffer (0.1 M) pH 7.1
Particles for evaluation of core/shell ratios PMMA-*co*-ALMA@PEA-*co*-PMEMO Throughout the polymerization, samples with different core/shell ratios are taken regularly for further investigations	44.36 g water 26 g EA 14 g MEMO 110 mg SDS 110 mg Dowfax 2A1 1.5 mL phosphate buffer (0,1 M) pH 7.1

General procedure for melt-shear organization

For film preparation, the resulting latex is lyophilized and the resulting powder is used for melt-shear organization. 2 g of the particle powder is given between two polyethylene terephthalate (PET) foils and immediately melt-sheared in a Collin laboratory press (P200 P/M) at different temperatures and pressures with an optimum at 140 °C and 180 bar. After 3 min, the press is opened and the colloidal crystal disk film is removed.

Characterization

Transmission electron microscopy (TEM) investigations were carried out on a Zeiss EM 10 electron microscope operating at 60 kV. All shown images were recorded with a slow-scan CCD camera obtained from TRS (Tröndle) in bright field mode. Camera control was computer-aided using the ImageSP software from TRS. Ultra-thin sections were prepared out of the bulk colloidal crystal film (overall thickness of 300–500 µm) using a Leica Ultracut UCT ultramicrotome yielding thin slices of 50 nm thickness. Dynamic light scattering (DLS) measurements were taken on a Zetasizer Nano

ZS90 (Malvern). For Scanning electron microscopy (SEM), a FEI/Philips XL30 FEG with accelerating voltages between 10 and 30 kV was used. The SEM samples were coated with gold for 120 s at 30 mA using a Quorum Q300T D sputter coater. For thermogravimetric analysis (TGA), a Mettler TGA2 was used in the temperature range from 35 to 600 °C with a heating rate of 10 K min^{-1} under oxygen or nitrogen atmosphere. The long-term thermal treatment was performed at 280 °C for 40 h with a heating rate of 10 K min^{-1}. Pyrolysis GC/MS was performed on Shimadzu GCMS-QP2010 Plus with an Ultra-alloy 5 (Frontier Lab) column under helium flow. The samples were pyrolyzed with a Frontier Lab PY-2020iD at 350 and 440 °C.

Results and discussion

Synthesis of MEMO-containing core/shell particles

Starved-feed emulsion polymerization was used for the preparation of hybrid core/shell particles with poly(methyl methacrylate-*co*-allyl methacrylate) (P(MMA-*co*-ALMA)) as core particles and shell material consisting of either poly(3-methacryloxypropyl-trimethoxysilane) (PMEMO) or alkoxysilane derivatives and poly(ethyl acrylate) (PEA) (Fig. 1).

In general, the synthesis of MEMO-containing particles has been only partially investigated in literature [43] and mostly miniemulsion polymerization strategies are described [44, 45]. In order to prevent early crosslinking through alkoxysilane moieties during starved-feed emulsion polymerization, the dispersions are buffered to pH = 7. As acidic byproducts during the initiator decomposition were typically formed, usage of a buffer system was mandatory. For this reason, a hydrogenphosphate/dihydrogenphosphate buffer system was used to maintain a constant pH during the polymerization. After particle synthesis, in order to avoid significant crosslinking during drying, the particles were lyophilized. Dried particles can be processed using the melt-shear technique to produce a hybrid core/shell particle film (see Scheme 1).

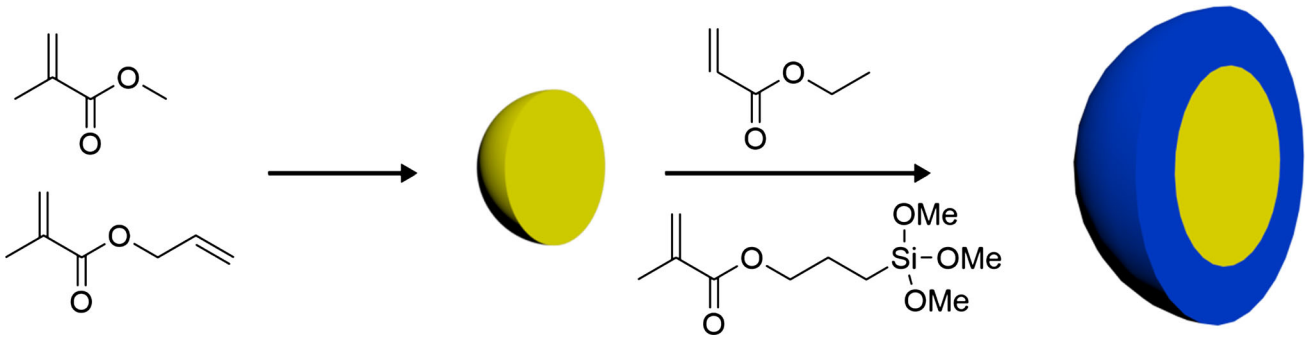

Figure 1 Particle synthesis starting from methyl methacrylate and allyl methacrylate as core material and ethyl acrylate and 3-methacryloxypropyl-trimethoxysilane as shell material.

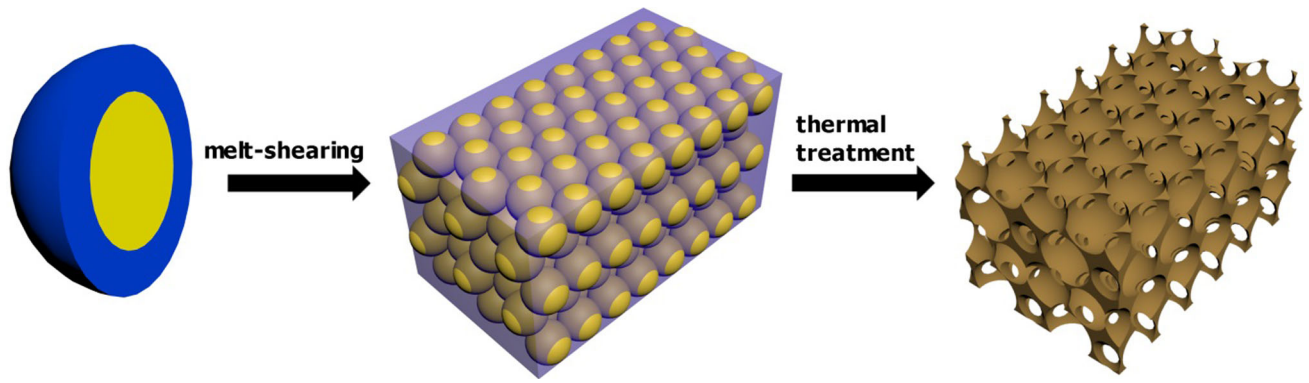

Scheme 1 Synthesis starting from core/shell particles to the melt-shear processed colloidal crystal film and subsequent removal of the cores via thermal treatment.

Removal of the template was achieved by thermal treatment of the hybrid films under optimized conditions after thorough investigation. As monodisperse particles are a basic prerequisite for application of the melt-shear organization technique as well as to obtain tailored porous inverse colloidal crystal films, perfectly adjusted particles in terms of size, dispersity and core/shell ratio had to be synthesized. For this purpose, starved-feed emulsion polymerization was conducted. The cores consist of poly(methyl methacrylate-*co*-allyl methacrylate) (P(MMA-*co*-ALMA)), since this copolymer degrades thermally at convenient temperatures [46–48] and the core material is partially crosslinked for the later use in the melt-shear process. Poly(ethyl acrylate) (PEA) copolymerized with MEMO was used as soft shell material [37, 49]. ALMA acts as anchor groups at the PMMA particles due to the different reactivities of the allyl groups compared to the methacrylic groups. Due to the presence of ALMA anchoring groups, a separation of the soft PMEMO-*co*-PEA-containing shell from the core particles was circumvented. The MEMO content was adjusted between 35 and 50 wt% with respect to a good balance of processability and significant ceramic yield after thermal treatment. A lower MEMO content leads to processable materials, but no porous structures were obtained due to high material loss. This can be explained by the decreasing degradation stability of shell material at low MEMO contents leading to unstable porous structures. As investigated by TGA (Figure S1), the thermal stability of the shell material is rather low for a MEMO content 10 wt%. The thermal stability significantly increases with increasing MEMO content, *i.e.*, for a content of 35 or 50 wt%, respectively. On the other hand, a high content of MEMO as shell material could not be processed via the melt-shear organization technique.

For tailoring the core/shell ratio, starved-feed ratio starved-feed emulsion polymerization was adapted as described in the experimental section. Due to the continuous addition of monomer emulsion in the starved-feed mode, the shell thickness successively increased with time. For investigating the optimal core/shell ratio, particle samples were taken from the reaction vessel and evaluated by TEM imaging and DLS measurements (Figure S2 and Table S1). The calculated core/shell ratios are based on the volume of an ideal sphere depending on the amount of added monomer emulsion and the speed of monomer addition with reaction time. The results of the particle sizes as determined by DLS measurements are in good agreement with the calculated core/shell ratios. In Fig. 2, exemplary TEM images of the PMMA-*co*-ALMA@PEA-*co*-PMEMO particles with a core shell ratio of 61:39 vol% are displayed. Additional TEM images of other samples can be found in the supporting information (Figure S3).

Concluding from these images, monodisperse core/shell particles with adjustable ratio of PMMA-*co*-ALMA core to PMEMO-*co*-PEA shell were accessible by the applied synthetic protocols. As required for melt-shear organization, the shell of the particles connects with each other forming a film due to the presence of soft PEA. Moreover, the obtained core/shell particles were uniform, which is a further

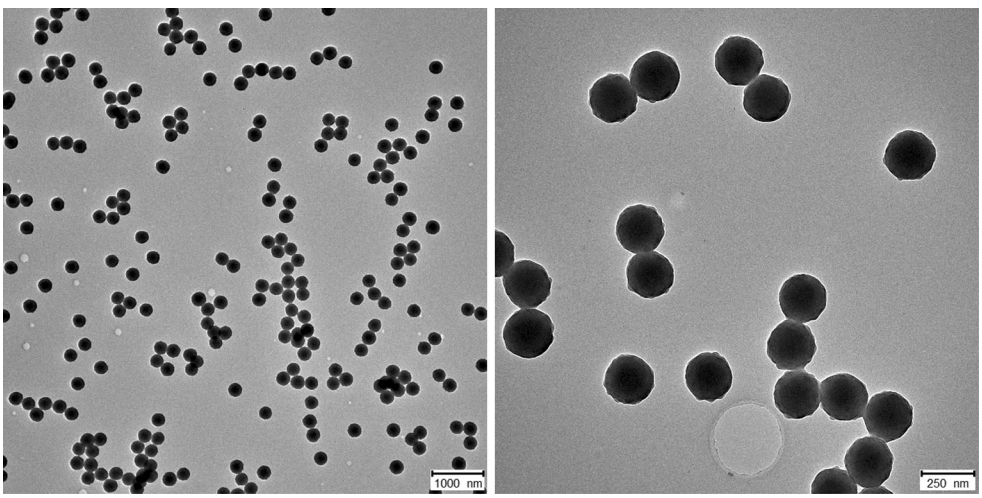

Figure 2 TEM images of monodisperse core/shell particles after synthesis via starved-feed emulsion polymerization.

prerequisite for colloidal crystal film formation as well as for the formation of isoporous structures which will be described in the ensuing sections [50]. The obtained core/shell materials were subsequently introduced into melt-shear processing.

Melt-shear organization for hybrid core/shell particles

The PMEMO-based core/shell particles featuring different core/shell ratios were investigated with respect to their usability in melt-shear organization and for the formation of porous materials. For this purpose, the experimental results regarding particle size and core/shell ratios played a crucial role in optimizing the organization process and the intended porosity of the final ceramic material. Prior to processing, the obtained particle suspension was lyophilized instead of using a more common drying process at elevated temperatures. This lyophilization step was necessary to obtain a dry particle powder featuring only small amounts of crosslinked alkoxysilanol moieties resulting in a processable material. In previous studies, the particle suspension was aggregated and dried followed by extrusion to enable the intended melt-shear processing. These additional steps ensure a homogenization of the particle powder, and additional additives comprising crosslinkers, radical crosslinking initiators as well as additives for increasing optical performance can be added. The resulting polymer strands were then processed via melt-shearing. Compared to previous studies applying multi-step procedures for colloidal crystal film formation, the herein presented MEMO-containing core/shell particles feature the advantage for direct colloidal crystal film formation due to their intrinsic capability of crosslinking reactions caused by the alkoxysilanol moieties. For this purpose, the lyophilized powder was homogenously distributed between two sheets of PET foil and processed via melt-shearing using a laboratory press. Exemplarily, in Fig. 3, the melt-sheared core/shell particle film of a lyophilized sample (left) and an oven-dried sample (right) are directly compared.

The obvious optical difference with respect to transparency between the two films was a result of the differences in sample preparation and processing. It can be concluded that the lyophilized, non-processed particles enabled the successful formation of transparent colloidal crystal films. In contrast, the film obtained from oven-dried powder was brittle due to unwanted crosslinking prior to melt-shear processing. For further optimization of processing parameters, the synthesized core/shell particles were processed under various conditions. In the following section, the influence of temperature and pressure on melt-shear processing was investigated. Figure 4 shows films processed at different temperatures for 3 min at a constant pressure of 180 bar.

As shown in Fig. 4, a processing temperature of 140 °C resulted in a clear and homogenously distributed hybrid polymer film. At lower temperatures, the film cannot flow freely and a turbid film was received. For temperatures higher than 140 °C, the fully melted and optically clear parts of the film decreased with increasing temperature and at 200 °C a continuous white film was obtained. A possible explanation for this behavior is the preferred condensation reaction of PMEMO at higher temperatures leading to a crosslinked and no longer processable material. Besides the temperature dependency, the influence of pressure on the resulting films is

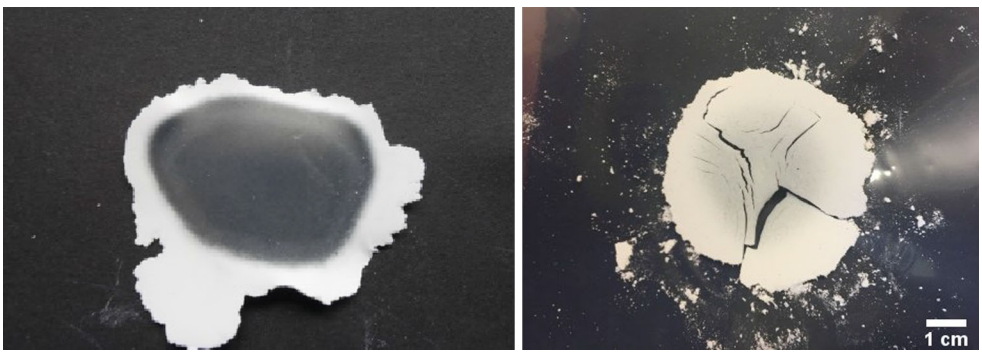

Figure 3 Photographs of the melt-sheared core/shell particle film of a lyophilized (*left*) and oven-dried powder (*right*). The *scalebar* corresponds to 1 cm.

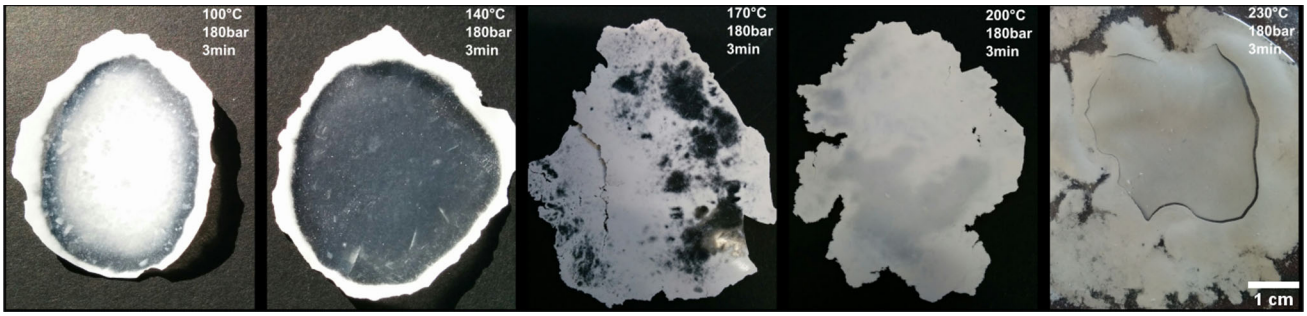

Figure 4 Photographs of the melt-sheared core–shell particle films processed at five different temperatures. The *scalebar* corresponds to 1 cm.

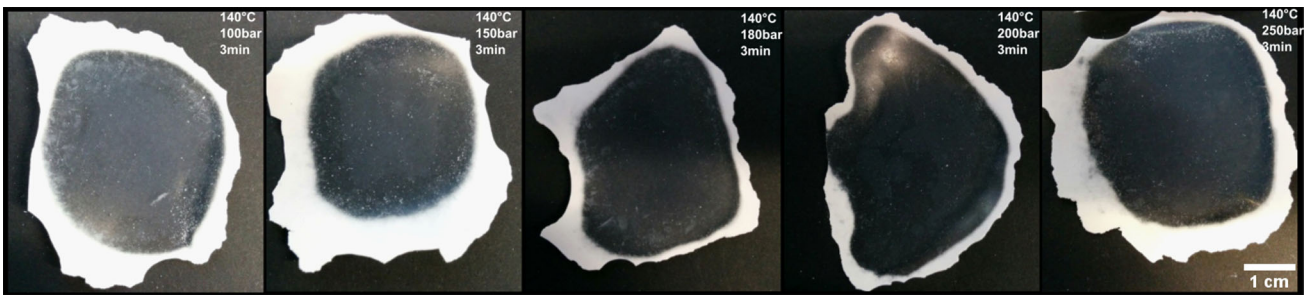

Figure 5 Photographs of the colloidal crystal films after melt-shear processing of core/shell particles under varying pressures. The *scalebar* corresponds to 1 cm.

investigated as well. The obtained films, melt-sheared for 3 min at 140 °C under varying pressures between 100 and 250 bar, are displayed in Fig. 5.

As can be concluded from these images by investigating the optical transparency and uniformity over the whole film with the naked eye, the variation of pressure had a minor influence on transparency and uniformity of the core/shell particle films. In all samples, the center of the film flowed freely becoming transparent because of the low refractive index contrast between core and shell. However, the samples prepared using 100–150 bar revealed a large white and cloudy boundary area of the colloidal crystal film which is reduced with increasing pressure. At pressures higher than 180 bar, the hybrid film became inhomogeneous and lost its smooth surface developing a rippled surface.

Furthermore, the core/shell ratio of the particles dramatically influences the processability: A thick shell is generally preferred for sufficient processability; however, this hinders the gaseous components to leave the interior of the film during thermal treatment bursting them. For this reason, the core/shell ratio had to be adjusted near the packing density of an ideal close-packed lattice (ratio 74 to 26 per volume). This correlates with the maximum packing fraction of the crosslinked PMMA-*co*-ALMA spheres, while the voids are filled with the shell material. For direct comparison of the processing capabilities, samples were taken continuously during the emulsion polymerization and then processed via melt-shearing in a subsequent step. Each sample taken at another reaction time correlates with a specific core/shell ratio. Samples from such a series are shown in Fig. 6 after melt-shearing.

The core/shell ratio obtained between 73:27 and 60:40 vol% had only a minor influence on processability leading to the most homogeneous film with a core/shell ratio of 66:34 vol%. Noteworthy, the higher core/shell ratios are in good correlation with the theoretical ratio of 74:26 vol%. Starting with a core/shell ratio of 64:36 vol% and higher shell thicknesses, all sample revealed an opaque boundary area surrounding the clear transparent film in the middle. A possible reason is the inhomogeneous distribution of the polymer due to a low flow rate at the outer edges and therefore loss of sufficient meltable material.

For the films prepared from the particle samples with 71:29 and 60:40 vol%, ultra-thin sections were

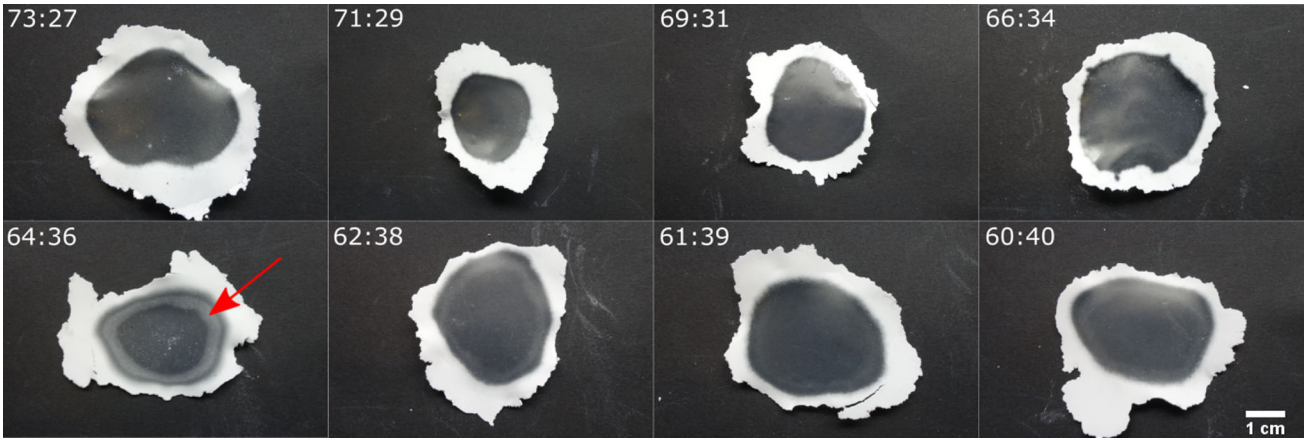

Figure 6 Photographs of the melt-shear processed particles with different core/shell ratios (see text). The *scalebar* corresponds to 1 cm.

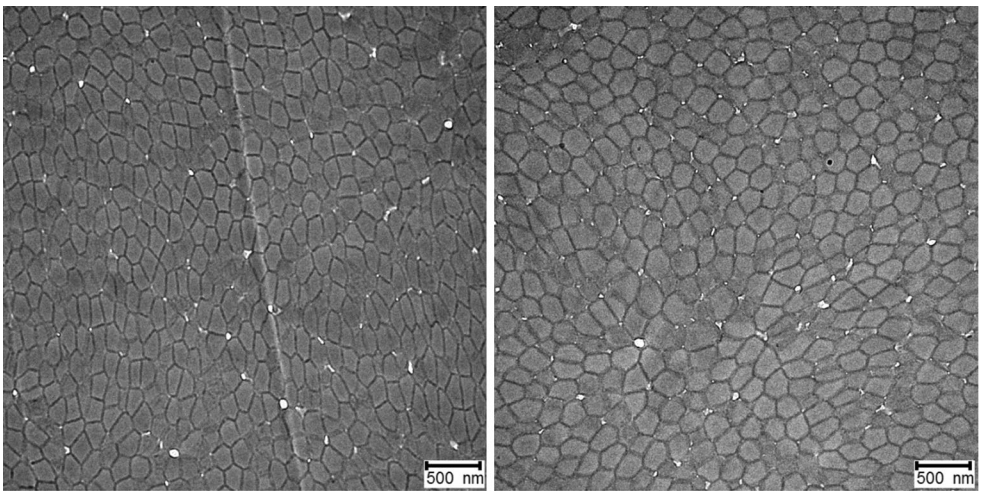

Figure 7 TEM images from ultra-thin sections of the processed films derived from the 71:29 vol% particle sample (*left*) and 60:40 vol% particle sample (*right*). *Scale bars* correspond to 500 nm.

prepared by using a ultramicrotome (see instrumentation section). The samples for ultramicrotomy were taken from the transparent part of the film, and the thin section was taken from the cross section of the particle film. TEM images of the ultra-thin sections are shown in Fig. 7.

The ultra-thin sections revealed a deformation of the particles inside both films. The crosslinked core remained intact but was soft enough to be deformed during melt-shear organization. However, the particles in the film with a thinner shell (left) were more deformed than the particles from the film with the thicker shell (right). The shell material interconnected the particles in order to produce a continuous matrix phase and therefore provides the possibility to create continuous porous networks. This will be further

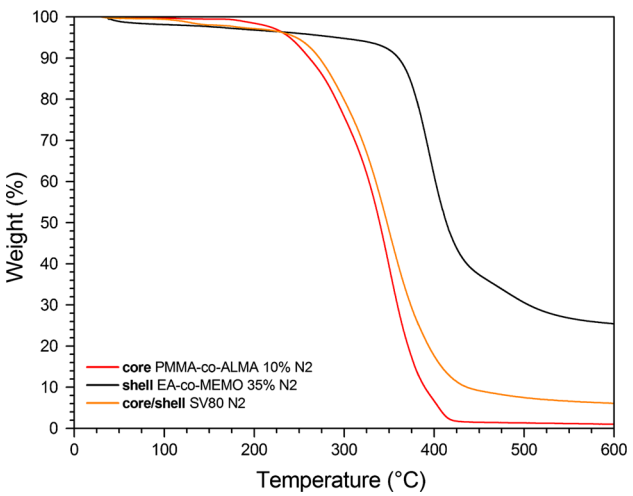

Figure 8 TGA of core (*red*), shell (*black*) and hybrid core–shell material (*orange*) in an atmosphere of nitrogen.

investigated via thermal treatment in the ensuing section.

Thermal degradation

In this section, thermal treatment of particles and colloidal crystal films was investigated in order to evaluate the feasibility of converting obtained hybrid polymer films into porous structures. As already mentioned above, PMMA was used as core material due to its capability for convenient thermal degradation. This feature was advantageously used to avoid the more common dissolution or etching protocols to obtain a porous network. The degradation behavior was investigated by thermogravimetric analysis (TGA). In Fig. 8, the degradation of pure core, complex core/shell and pure shell materials is compared.

As can be drawn from TGA results, the degradation of P(MMA-*co*-ALMA) core material started at considerably lower temperature than the degradation of pure shell material, which was derived from a starved-feed emulsion polymerization with a PMEMO content of 35%. The degradation curve of the hybrid core/shell material was nearly identical to the degradation curve of the core material. Therefore, it is assumed that primarily the core material was removed by thermal treatment. TGA proved the possibility to degrade the core material prior to decomposition of the shell material. Furthermore, the high MEMO content (35–50%) in the particle shell induces crosslinking reaction and, thus, leads to a significantly higher ceramic yield of around 10–15% compared to low MEMO content (10%). The mechanism of degradation concluded from TGA was additionally supported by pyrolysis gas chromatography/mass (GC/MS) spectrometry measurements (Figure S4 and S5). From these measurements, it can be concluded that the shell material has an increased degradation temperature. Additionally the main degradation products observed were the monomers, ethylene, ethanol, CO_2 and H_2O.

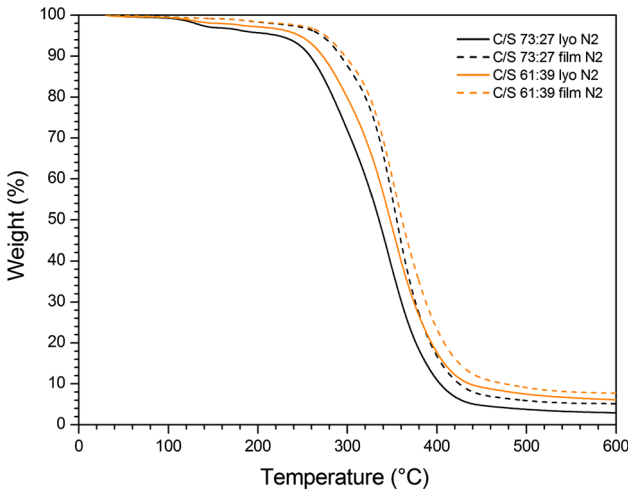

Figure 9 TGA of the lyophilized powder and the melt-sheared film with core/shell ratios of 73:27 and 61:39.

Another interesting aspect is the influence of the core/shell ratio on the degradation and the difference between lyophilized powder and the melt-sheared film. This was investigated by TGA measurements (Fig. 9). The two compared core/shell particles (PMMA-*co*-ALMA@PEA-*co*-PMEMO) samples featured a core shell ratio of 73:27 as thin shell and 61:39 as thick shell.

The difference between the two solid lines that corresponds to the difference in core/shell ratio revealed that the particle powder featuring a thicker shell was slightly shifted to higher degradation temperatures with a difference of approx. 15 °C. Likewise a similar shift was observed for the melt-sheared film in comparison with the lyophilized powder. The difference here was only 5 °C. This leads to the conclusion that the degradation was diffusion limited in the powder, and especially in the melt-sheared film, the decomposed material cannot leave the interior of the particle film. For this reason, thermal treatment protocols for the degradation of PMMA core materials were conducted at low temperatures (280 °C) for a prolonged time (40 h). Exemplary SEM images of the porous hybrid particle film after thermal treatment are shown in Fig. 10. These optimized conditions at low temperatures lead to a partial degradation of the shell material and a significant degradation of the template core material. As a result, the matrix-forming shell material is maintained resulting in a stable uniform porous structure.

The SEM images of the colloidal crystal film made from PMMA-*co*-ALMA@PEA-*co*-PMEMO particles with a core shell ratio of 73:27 revealed homogenously distributed open pores over a wide area of the film with graphically obtained pore sizes of 53 ± 13 nm. The obtained core/shell ratio is near the expected theoretical ratio of 74:26 of the maximum packing fraction of hard spheres. The mild thermal treatment was therefore a suitable method to create porous structures. The partial degradation has the

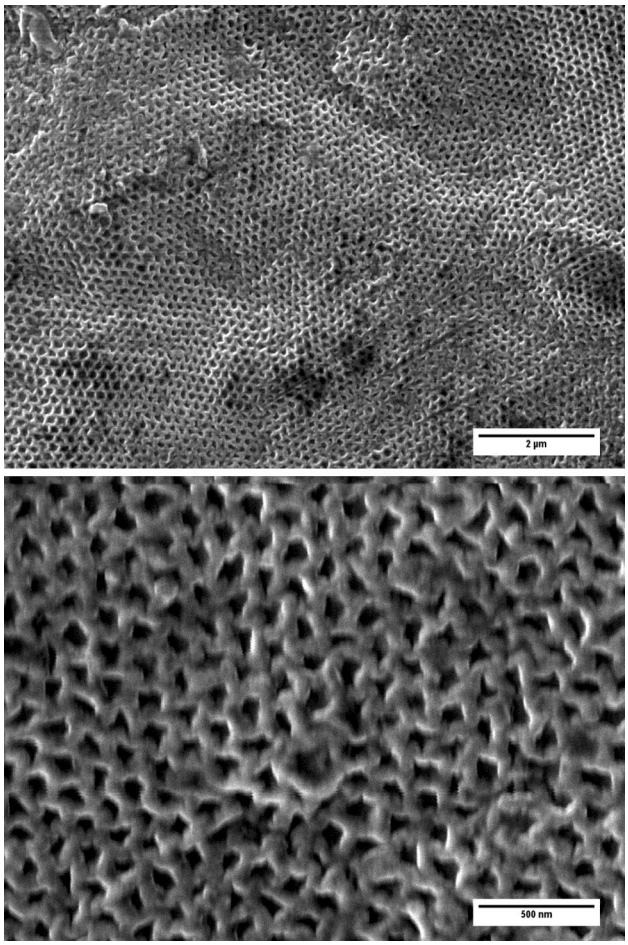

Figure 10 SEM images of the thermally treated film at 280 °C, 40 h under nitrogen. The *scalebar* corresponds to 2 µm (*top*) and 500 nm (*bottom*).

advantage that a porous material is obtained while the mechanical stability of a polymeric material remains.

Conclusions

Starved-feed emulsion polymerization for the preparation of hybrid core/shell particles consisting of poly(methyl methacrylate-*co*-allyl methacrylate) (P(MMA-*co*-ALMA)) core and a poly(ethyl acrylate-*co*-(3-methacryloxypropyl-trimethoxysilane)) (PEA-*co*-PMEMO) shell was successfully applied. Monodisperse hybrid core/shell particles were obtained providing access to porous materials after thermal treatment. The crosslinking strategy via siloxane moieties as part of the soft copolymer particle shell was investigated. During particle synthesis, self-crosslinking was avoided by using a suitable pH buffer system. The core/shell particles were investigated by TEM and DLS measurements proving that monodisperse hybrid particles were obtained due to the excellent reaction control. The core/shell particles were processed by the melt-shear organization technique allowing the soft shell for the formation of a hybrid siloxane-containing matrix with embedded and well-distributed PMMA particles. The siloxane crosslinking during this processing step was shown to increase the thermal stability of the matrix material. This offers the capability of the template removal via thermal treatment. To obtain a mechanically stable material featuring a porous structure, thermal treatment had to be performed under comparably mild conditions for a prolonged time (280 °C, 40 h). This convenient strategy based on novel self-crosslinkable core/shell particles and processing by melt-shear organization to colloidal crystal films will pave the way to porous hybrid materials after thermal treatment. These porous free-standing film materials are potential candidates for hybrid membranes and catalyst supports.

Acknowledgements

S.V. thanks the Evangelisches Studienwerk Villigst and the Max-Buchner Foundation for financial support. M.G. would like to thank the Fonds der Chemischen Industrie and the LOEWE project iNAPO by the Hessen State Ministry of Higher Education for partial financial support of this work. M.G. additionally acknowledges the German Research Foundation (DFG GA 2169/5-1) for partial support of this work. This work has been additionally supported in the frame of the Smart Inorganic Polymer EU network (COST CM10302, SIPS).

Compliance with ethical standards

Conflict of interest The authors declare that they have no conflict of interest.

Electronic supplementary material: The online version of this article (doi:10.1007/s10853-017-0891-2) contains supplementary material, which is available to authorized users.

References

[1] Christodoulou L, Venables JD (2003) Multifunctional material systems: the first generation. JOM 55:39–45

[2] Davis ME (2002) Ordered porous materials for emerging applications. Nature 417:813–821

[3] Burda C, Chen X, Narayanan R, El-Sayed MA (2005) Chemistry and properties of nanocrystals of different shapes. Chem Rev 105:1025–1102

[4] Zhao Y, Jiang L (2009) Hollow micro/nanomaterials with multilevel interior structures. Adv Mater 21:3621–3638. doi:10.1002/adma.200803645

[5] Talapin DV, Lee J-S, Kovalenko MV, Shevchenko EV (2010) Prospects of colloidal nanocrystals for electronic and optoelectronic applications. Chem Rev 110:389–458

[6] Aissou K, Shaver J, Fleury G, Pecastaings G, Brochon C, Navarro C, Grauby S, Rampnoux JM, Dilhaire S, Hadziioannou G (2013) Nanoscale block copolymer ordering induced by visible interferometric micropatterning: a route towards large scale block copolymer 2D crystals. Adv Mater 25(2):213–217. doi:10.1002/adma.201203254

[7] Koo K, Ahn H, Kim S-W, Ryu DY, Russell TP (2013) Directed self-assembly of block copolymers in the extreme: guiding microdomains from the small to the large. Soft Matter 9(38):9059. doi:10.1039/c3sm51083b

[8] Orilall MC, Wiesner U (2011) Block copolymer based composition and morphology control in nanostructured hybrid materials for energy conversion and storage: solar cells, batteries, and fuel cells. Chem Soc Rev 40:520–535

[9] She M-S, Lo T-Y, Hsueh H-Y, Ho R-M (2013) Nanostructured thin films of degradable block copolymers and their applications. NPG Asia Mater 5:e42

[10] Ren Y, Ma Z, Bruce PG (2012) Ordered mesoporous metal oxides: synthesis and applications. Chem Soc Rev 41:4909–4927

[11] Innocenzi P, Malfatti L (2013) Mesoporous thin films: properties and applications. Chem Soc Rev 42:4198–4216

[12] Petkovich ND, Stein A (2013) Controlling macro- and mesostructures with hierarchical porosity through combined hard and soft templating. Chem Soc Rev 42:3721–3739

[13] Rawolle M, Niedermeier MA, Kaune G, Perlich J, Lellig P, Memesa M, Cheng YJ, Gutmann JS, Müller-Buschbaum P (2012) Fabrication and characterization of nanostructured titania films with integrated function from inorganic-organic hybrid materials. Chem Soc Rev 41:5131–5142

[14] Whitesides GM (2005) Nanoscience, nanotechnology, and chemistry. Small 1(2):172–179

[15] Piao Y, Burns A, Kim J, Wiesner U, Hyeon T (2008) Designed fabrication of silica-based nanostructured particle systems for nanomedicine applications. Adv Funct Mater 18:3745–3758

[16] Schüth F, Schmidt W (2002) Microporous and mesoporous materials. Adv Mater 14:629–638

[17] Stein A (2003) Advances in microporous and mesoporous solids—highlights of recent progress. Adv Mater 15:763–775

[18] Thomas A, Goettmann F, Antonietti M (2008) Hard templates for soft materials: creating nanostructured organic materials. Chem Mater 20:738–755

[19] Llusar M, Sanchez C (2008) Inorganic and hybrid nanofibrous materials templated with organogelators. Chem Mater 20:782–820

[20] Joshi RK, Schneider JJ (2012) Assembly of one dimensional inorganic nanostructures into functional 2D and 3D architectures. Synthesis, arrangement and functionality. Chem Soc Rev 41:5285–5312. doi:10.1039/c2cs35089k

[21] Scheid D, Cherkashinin G, Ionescu E, Gallei M (2014) Single-source magnetic nanorattles by using convenient emulsion polymerization protocols. Langmuir 30(5):1204–1209

[22] Lou XW, Archer LA, Yang Z (2008) Hollow micro-/nanostructures: synthesis and applications. Adv Mater 20:3987–4019. doi:10.1002/adma.200800854

[23] Ge J, Yin Y (2011) Responsive photonic crystals. Angew Chem Int Ed Engl 50:1492–1522

[24] Galisteo-López JF, Ibisate M, Sapienza R, Froufe-Pérez LS, Blanco Á, López C (2011) Self-assembled photonic structures. Adv Mater 23:30–69

[25] von Freymann G, Kitaev V, Lotsch BV, Ozin GA (2013) Bottom-up assembly of photonic crystals. Chem Soc Rev 42:2528–2554

[26] Schäfer CG, Vowinkel S, Hellmann GP, Herdt T, Contiu C, Schneider JJ, Gallei M (2014) A polymer based and template-directed approach towards functional multidimensional microstructured organic/inorganic hybrid materials. J Mater Chem C 2:7960–7975

[27] Pursiainen OLJ, Baumberg JJ, Winkler H, Viel B, Spahn P, Ruhl T (2008) Shear-induced organization in flexible polymer opals. Adv Mater 20:1484–1487

[28] Ruhl T, Spahn P, Hellmann GP (2003) Artificial opals prepared by melt compression. Polymer 44:7625–7634

[29] Finlayson CE, Spahn P, Snoswell DR, Yates G, Kontogeorgos A, Haines AI, Hellmann GP, Baumberg JJ (2011) 3D bulk ordering in macroscopic solid opaline films by edge-induced rotational shearing. Adv Mater 23:1540–15444

[30] Kontogeorgos A, Snoswell DRE, Finlayson CE, Baumberg JJ, Spahn P, Hellmann GP (2010) Inducing symmetry breaking in nanostructures: anisotropic stretch-tuning photonic crystals. Phys Rev Lett 105:233909

[31] Wong HS, Mackley M, Butler S, Baumberg J, Snoswell D, Finlayson C, Zhao Q (2014) The rheology and processing of

"edge sheared" colloidal polymer opals. J Rheol 58(2):397–409

[32] Zhao Q, Finlayson CE, Snoswell DRE, Haines A, Schäfer C, Spahn P, Hellmann GP, Petukhov AV, Herrmann L, Burdet P, Midgley PA, Butler S, Mackley M, Guo Q, Baumberg JJ (2016) Large-scale ordering of nanoparticles using viscoelastic shear processing. Nat Commun 7:11661

[33] Wang J, Zhang Y, Wang S, Song Y, Jiang L (2011) Bioinspired colloidal photonic crystals with controllable wettability. Acc Chem Res 44:405–415

[34] Yang D, Ye S, Ge J (2014) From metastable colloidal crystalline arrays to fast responsive mechanochromic photonic gels: an organic gel for deformation-based display panels. Adv Funct Mater 24:3197–3205

[35] Schäfer CG, Gallei M, Zahn JT, Engelhardt J, Hellmann GP, Rehahn M (2013) Reversible light-, thermo-, and mechano-responsive elastomeric polymer opal films. Chem Mater 25:2309–2318

[36] Schäfer CG, Smolin DA, Hellmann GP, Gallei M (2013) Fully reversible shape transition of soft spheres in elastomeric polymer opal films. Langmuir 29:11275–11283

[37] Schäfer CG, Viel B, Hellmann GP, Rehahn M, Gallei M (2013) Thermo-cross-linked elastomeric opal films. ACS Appl Mater Interfaces 5(21):10623–10632

[38] Schäfer CG, Lederle C, Zentel K, Stuhn B, Gallei M (2014) Utilizing stretch-tunable thermochromic elastomeric opal films as novel reversible switchable photonic materials. Macromol Rapid Commun 35(21):1852–1860

[39] Schäfer CG, Lederle C, Zentel K, Stühn B, Gallei M (2014) Utilising stretch-tunable thermochromic elastomeric opal films as novel reversible switchable photonic materials. Macromol Rap Commun 35(21):1852–1860

[40] Scheid D, Lederle C, Vowinkel S, Schäfer CG, Stühn B, Gallei M (2014) Redox- and mechano-chromic response of metallopolymer-based elastomeric colloidal crystal films. J Mater Chem C 2:2583–2590

[41] Schäfer CG, Winter T, Heidt S, Dietz C, Ding T, Baumberg JJ, Gallei M (2015) Smart polymer inverse-opal photonic crystal films by melt-shear organization for hybrid core–shell architectures. J Mater Chem C 3(10):2204–2214

[42] Vowinkel S, Schäfer CG, Cherkashinin G, Fasel C, Roth F, Liu N, Dietz C, Lonescu E, Gallei M (2016) 3D-ordered carbon materials by melt-shear organization for tailor-made hybrid core–shell polymer particle architectures. J Mater Chem C 4:3976–3986

[43] Ni K, Shan G, Weng Z, Sheibat-Othman N, Fevotte G, Lefebvre F, Bourgeat-Lami E (2005) Synthesis of hybrid core-shell nanoparticles by emulsion (co) polymerization of styrene and γ-methacryloxypropyltrimethoxysilane. Macromolecules 38(17):7321–7329

[44] Ni K-F, Shan G-R, Weng Z-X (2006) Synthesis of hybrid nanocapsules by miniemulsion (co) polymerization of styrene and γ-methacryloxypropyltrimethoxysilane. Macromolecules 39(7):2529–2535

[45] Zhang S-W, Zhou S-X, Weng Y-M, Wu L-M (2006) Synthesis of silanol-functionalized latex nanoparticles through miniemulsion copolymerization of styrene and γ-methacryloxypropyltrimethoxysilane. Langmuir 22(10):4674–4679

[46] Ferriol M, Gentilhomme A, Cochez M, Oget N, Mieloszynski J (2003) Thermal degradation of poly (methyl methacrylate)(PMMA): modelling of DTG and TG curves. Polym Degrad Stab 79(2):271–281

[47] Manring LE (1988) Thermal degradation of saturated poly (methyl methacrylate). Macromolecules 21(2):528–530

[48] Manring LE, Sogah DY, Cohen GM (1989) Thermal degradation of poly (methyl methacrylate). 3. Polymer with head-to-head linkages. Macromolecules 22(12):4652–4654

[49] Schäfer CG, Lederle C, Zentel K, Stühn B, Gallei M (2014) Utilizing stretch-tunable thermochromic elastomeric opal films as novel reversible switchable photonic materials. Macromol Rapid Commun 35(21):1852–1860

[50] Schäfer C, Winter T, Heidt S, Dietz C, Ding T, Baumberg J, Gallei M (2015) Smart polymer inverse-opal photonic crystal films by melt-shear organization for hybrid core–shell architectures. J Mater Chem C 3(10):2204–2214